Transactions of the Materials Research Society of Japan Vol.28 7-10 (2003)

Quantitative Evaluation for Grazing Incidence X-Ray Scattering Data

Kazuhiko Omote and Yoshiyasu Ito
X-Ray Research Laboratory, Rigaku Corporation, Tokyo 196-8666, Japan
Fax: 81-42-546-7093, e-mail: omote@rigaku.co.jp

For determining nanostructure by grazing incidence x-ray scattering data quantitatively, we have considered Reflection and refraction at the surface and film interfaces based on distorted wave Born approximation. In addition, we also taken into account diffuse scattering by the surface and interface roughness together with scattering from the nanostructure at the surface and/or inside the layers. Small-angle x-ray scattering data must be analyzed by employing appropriate models for the nanostructures. Some possible models are discussed. The present technique has been applied for determining pore-size distribution in porous low-κ dielectric films. The resulting size and distributions are compared to that of other techniques, the N_2 gas adsorption.

Key words: Grazing incidence, Small angle x-ray scattering, DWBA, Pore size distribution, Low-κ dielectric film

1. INTRODUCTION

In recent years, there has been considerable interest in the research and development of nanostructural materials constructed on the surface and/or inside the thin film layers. For example, quantum dots and wires on the semiconductor surfaces, nanoporous low-κ dielectric films, granular magnetic thin films, and so on. By using such kinds of nanostructures, we can control electric, magnetic, physical, and chemical properties of thin films. Such properties are very close related to the size, shape, size-distribution, and correlation of the nanostructures. X-ray scattering is very useful for determining such nanostructures, quantitatively and nondestructively. X-ray scattering patterns can be calculated for film structures by using an established scattering theory, and the observed scattering data can be analyzed quantitatively. In addition, x-ray photons can penetrate inside the film materials without serous radiation damages.

When we use grazing incidence geometry as seen in Fig. 1, however, we have to deal with reflection and refraction of x-rays at the surface and interfaces correctly in order to determine nanostructure quantitatively. We, therefore, have calculated x-ray scattering intensities for the grazing incidence geometry based on the distorted wave Born approximation (DWBA) [1, 2].

Furthermore, we must employ appropriate models suited for the structural characteristics of the nanostructures. We, therefore, will discuss some typical structural models for analyzing x-ray scattering patterns. Finally, we will present an example, which we determined pore size distribution of porous low-κ dielectric films.

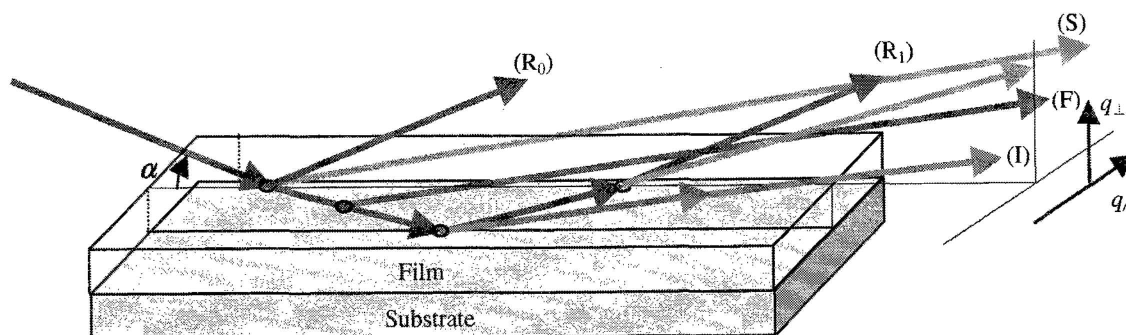

Fig. 1. Reflection, refraction, and scatterings at the surface, interfaces, and inside the film layers. (R_0) and (R_1): Specular reflection at the surface and interface. (F): Scattering inside the film layers. (S): Scattering at the film surface. (I): Scattering at the interfaces.

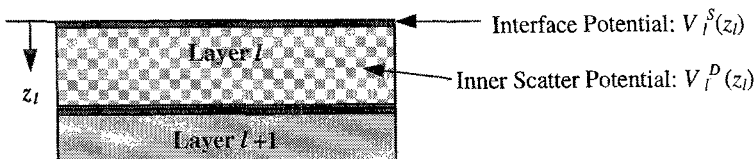

Fig. 2. The scattered potential at the surface and interface V^S and inside the layers V^D.

2. CALCULATION METHOD

Reflection and transmitted coefficients $R_l(\alpha)$ and $T_l(\alpha)$ of the l th layer with the incident angle α can be calculated by the Fresnel's formula. X-ray wave field $E_l(\alpha, z_l)$ in the film at the depth z_l is written as[3]

$$R_N = 0,\quad R_{N-1} = \gamma_{N-1},\quad \cdots,\quad R_l = \frac{R_{l+1}\varphi_{l+1}^{\;2} + \gamma_l}{R_{l+1}\varphi_{l+1}^{\;2}\gamma_l + 1}, \qquad R_0 = \frac{R_1\varphi_1^{\;2} + \gamma_0}{R_1\varphi_1^{\;2}\gamma_0 + 1} \tag{1}$$

$$\eta_l = \sqrt{n_l - \cos^2\alpha},\quad \gamma_l = \frac{\eta_l - \eta_{l+1}}{\eta_l + \eta_{l+1}},\quad \tau_l = \frac{2\eta_{l+1}}{\eta_l + \eta_{l+1}}, \qquad \varphi_l = e^{ik_0\eta_l \cdot d_l},\quad t_l = \frac{1-\gamma_l R_l}{\tau_l} \tag{2}$$

$$^{T}E_l(z_l) = \prod_{j=1}^{l-1}\left(t_j\varphi_j\right)e^{ik_0\eta_l z_l}, \qquad ^{R}E_l(z_l) = \prod_{j=1}^{l-1}\left(t_j\varphi_j\right)\left(R_l\varphi_l^{\;2}\right)e^{-ik_0\eta_l z_l} \tag{3}$$

Where k_0 is wave vector of the incident x-ray, d_l thickness of the film, n_l refractive index of the l-th layer. The scattered wave can be represented by a time reversal state of the incoming wave[2]. Therefore, the scattered wave field $\tilde{E}_l(\beta, z_l)$ in the film with the exit angle β can be written the same way as the above equations by using the time reversal state,

$$\tilde{R}_N^{\;*} = 0,\quad \tilde{R}_{N-1}^{\;*} = \tilde{\gamma}_{N-1}^{\;*},\quad \cdots, \qquad \tilde{R}_l^{\;*} = \frac{\tilde{R}_{l+1}^{\;*}\tilde{\varphi}_{l+1}^{\;*2} + \tilde{\gamma}_l^{\;*}}{\tilde{R}_{l+1}^{\;*}\tilde{\varphi}_{l+1}^{\;*2}\tilde{\gamma}_l^{\;*} + 1},\quad \tilde{R}_0^{\;*} = \frac{\tilde{R}_1^{\;*}\tilde{\varphi}_1^{\;*2} + \tilde{\gamma}_0^{\;*}}{\tilde{R}_1^{\;*}\tilde{\varphi}_1^{\;*2}\tilde{\gamma}_0^{\;*} + 1}, \tag{4}$$

$$\zeta_l = \sqrt{n_l - \cos^2\beta},\quad \tilde{\gamma}_l^{\;*} = \frac{\zeta_l^{\;*} - \zeta_{l+1}^{\;*}}{\zeta_l^{\;*} + \zeta_{l+1}^{\;*}},\quad \tilde{\tau}_l^{\;*} = \frac{2\zeta_{l+1}^{\;*}}{\zeta_l^{\;*} + \zeta_{l+1}^{\;*}}, \qquad \tilde{\varphi}_l^{\;*} = e^{-ik_0\zeta_l^{\;*} d_l},\quad \tilde{t}_l^{\;*} = \frac{1-\tilde{\gamma}_l^{\;*}\tilde{R}_l^{\;*}}{\tilde{\tau}_l^{\;*}} \tag{5}$$

$$^{T}\tilde{E}_l(z_l) = \prod_{j=1}^{l-1}\left(\tilde{t}_j^{\;*}\tilde{\varphi}_j^{\;*}\right)e^{-ik_0\zeta_l^{\;*} z_l}, \qquad ^{R}\tilde{E}_l(z_l) = \prod_{j=1}^{l-1}\left(\tilde{t}_j^{\;*}\tilde{\varphi}_j^{\;*}\right)\left(\tilde{R}_l^{\;*}\tilde{\varphi}_l^{\;*2}\right)e^{ik_0\zeta_l^{\;*} z_l}. \tag{6}$$

By using the above expressions, incident and scattered electric wave fields $\psi_i(\alpha)\big|_l$ and $\psi_f(\alpha)\big|_l$, respectively, in l-th layer can be written as

$$\psi_i(\alpha)\big|_l = T_l e^{ik_0\eta_l z_l} + T_l R_l \varphi_l^{\;2} e^{-ik_0\eta_l z_l}, \qquad \tilde{\psi}_f(\beta)\big|_l = \tilde{T}_l^{\;*} e^{-ik_0\zeta_l^{\;*} z_l} + \tilde{T}_l^{\;*}\tilde{R}_l^{\;*}\tilde{\varphi}_l^{\;*2} e^{ik_0\zeta_l^{\;*} z_l}, \qquad T_l = \prod_{j=1}^{l-1}\left(t_j\varphi_j\right),\quad \tilde{T}_l^{\;*} = \prod_{j=1}^{l-1}\left(\tilde{t}_j^{\;*}\tilde{\varphi}_j^{\;*}\right) \tag{7}$$

We consider two types of scatter potentials in this paper; one is caused by interface roughness V^S and the other nanostructures inside the layers V^D as shown in Fig. 2. Transition amplitude by these potentials can be written in first order DWBA as follows.

$$T_{fi} = \frac{1}{4\pi}\left\langle \tilde{\psi}_f \middle| V \middle| \psi_i \right\rangle = \frac{1}{4\pi}\sum_l \begin{bmatrix} \tilde{T}_l T_l \left\langle -\zeta_l^{\;*} \middle| V_l^S + V_l^D \middle| \eta_l \right\rangle \\ +\tilde{T}_l \tilde{R}_l \tilde{\varphi}_l^{\;2} T_l \left\langle \zeta_l^{\;*} \middle| V_l^S + V_l^D \middle| \eta_l \right\rangle \\ +\tilde{T}_l T_l R_l \varphi_l^{\;2} \left\langle -\zeta_l^{\;*} \middle| V_l^S + V_l^D \middle| -\eta_l \right\rangle \\ +\tilde{T}_l \tilde{R}_l \tilde{\varphi}_l^{\;2} T_l R_l \varphi_l^{\;2} \left\langle \zeta_l^{\;*} \middle| V_l^S + V_l^D \middle| -\eta_l \right\rangle \end{bmatrix} \tag{8}$$

If we assume interference terms between V^S and V^D can be neglected and the V^D is randomly distributed inside the film and the frequently oscillated thickness fringes are ignored, the transition probability of these two states can be calculated for inside the layers,

$$\begin{aligned} \left|T^D{}_{fi}\right|^2 = r_e^{\;2}\sum_l \Delta\rho_l^2 N_l \Bigg[& \left|\tilde{T}_l T_l\right|^2 \left|F_l(q^+)\right|^2 \frac{1-e^{-2k_0 \operatorname{Im}(\eta_l+\zeta_l)d_l}}{2k_0 \operatorname{Im}(\eta_l+\zeta_l)} + \left|\tilde{T}_l \tilde{R}_l T_l\right|^2 \left|F_l(q^-)\right|^2 e^{-4k_0 \operatorname{Im}\zeta_l d_l} \frac{1-e^{-2k_0 \operatorname{Im}(\eta_l-\zeta_l)d_l}}{2k_0 \operatorname{Im}(\eta_l-\zeta_l)} \\ & + \left|\tilde{T}_l T_l R_l\right|^2 \left|F_l(q^-)\right|^2 e^{-4k_0 \operatorname{Im}\eta_l d_l} \frac{1-e^{-2k_0 \operatorname{Im}(\zeta_l-\eta_l)d_l}}{2k_0 \operatorname{Im}(\zeta_l-\eta_l)} + \left|\tilde{T}_l \tilde{R}_l T_l R_l\right|^2 \left|F_l(q^+)\right|^2 e^{-4k_0 \operatorname{Im}(\zeta_l+\eta_l)d_l} \frac{e^{2k_0 \operatorname{Im}(\eta_l+\zeta_l)d_l}-1}{2k_0 \operatorname{Im}(\eta_l+\zeta_l)} \Bigg] \end{aligned} \tag{9}$$

and for the interfaces

$$\left|T^S{}_{fi}\right|^2 = r_e^{\;2}\left|\sum_l (\rho_{l-1}-\rho_l)\begin{bmatrix} \tilde{T}_l T_l F_l^S(q_\perp^{\;+}, q_{//}) + \tilde{T}_l \tilde{R}_l T_l F_l^S(q_\perp^{\;-}, q_{//}) e^{-2k_0 \operatorname{Im}\zeta_l d_l} \\ +\tilde{T}_l T_l R_l F_l^S(q_\perp^{\;-}, q_{//}) e^{-2k_0 \operatorname{Im}\eta_l d_l} + \tilde{T}_l \tilde{R}_l T_l R_l F_l^S(q_\perp^{\;+}, q_{//}) e^{-2k_0 \operatorname{Im}(\zeta_l+\eta_l)d_l} \end{bmatrix}\right|^2 \tag{10}$$

It should be noted that the scattering vectors are different for each processes,

$$\begin{cases} q^{+} = \sqrt{(q_{\perp}^{+})^{2} + (q_{//})^{2}} \\ q^{-} = \sqrt{(q_{\perp}^{-})^{2} + (q_{//})^{2}} \end{cases}, \quad \begin{cases} q_{\perp}^{+} = \mathrm{Re}[k_0(\eta_l + \zeta_l)] \\ q_{\perp}^{-} = \mathrm{Re}[k_0(\eta_l - \zeta_l)] \end{cases},$$
$$q_{//} = k_0(\cos\beta - \cos\alpha) \tag{11}$$

For calculating equation (10), Shnha[2] introduced a structure factor $S(q_{\perp}, q_{//})$ for the surface and interfaces

$$S_{\mathrm{interface}}(q) = \frac{2\pi}{q_{\perp}^{2}} e^{-q_{\perp}^{2}\sigma^{2}} \int_0^{\infty} dR\, R\, F(q_{\perp}, R) J_0(q_{//}R),$$
$$F(q_{\perp}, R) = \exp\left[q_{\perp}^{2}\sigma^{2} e^{-\left(\frac{R}{\xi}\right)^{2h}} \right] - 1 \tag{12}$$

Where h is the fractal parameter, ξ lateral correlation length, and σ rms roughness. Other scattering models for the interface nanostructure have been also presented [4]. There are many possible models for calculating structure factor for the potential V^{D}. For example, Debye presented[5] a scattering function based on the random phase separation model.

$$I(q) = \frac{8\pi V_B(1 - V_B)\Delta\rho_{AB}^{2}\xi^{3}}{\left(1 + q^{2}\xi^{2}\right)^{2}}, \tag{13}$$

where $\Delta\rho_{AB}$ is the difference of the density of the materials A and B, V_B volume fraction of material B, and ξ correlation length of the phase separation. The simplest example of the form factor is for a sphere with radius R.

$$F(q, R) = \frac{4\pi R^{3}}{(qR)^{3}}\left[\sin(qR) - (qR)\cos(qR)\right] \tag{14}$$

And we can convolute different radius with appropriate distributions $f(R, R_{AV})$ with mean value R_{AV},

$$|F(q; R_{AV})|^{2} = \int_0^{\infty} f(R, R_{AV}) \left(\frac{R_{AV}}{R}\right)^{3} |r_e \rho F(q, R)|^{2} dR \tag{15}$$

We have employed Γ-distribution as $f(R, R_{AV})$ for analyzing pore size distribution in porous low-κ thin films[6], because of its flexibly of the shape and it is a distribution for the positive numerals. Cylinder, core-shell, etc. must be considered if the shape of the nanostructure is obvious. In addition, interference effects are sometimes become distinct when increasing the density of nanostructures. In such a case, we must introduce structure factor of the packing.

3. EXPERIMENTALS

Low-κ dielectric films are used in ultra-high density integrated circuits to avoid a delay of signal propagation and cross talks. An introduction of nanometer-sized pores into dielectric films reduces their dielectric constant. To estimate size and distribution of the pore are very important for the porous films. X-ray scattering measurements for porous low-κ thin films were made using a Rigaku ATX diffractometer[7] with rotating anode x-ray generator operated at 50 kV and 300 mA. Parallel and monochromatic Cu Kα radiation obtained by a parabolic graded multilayer mirror[8] was used.

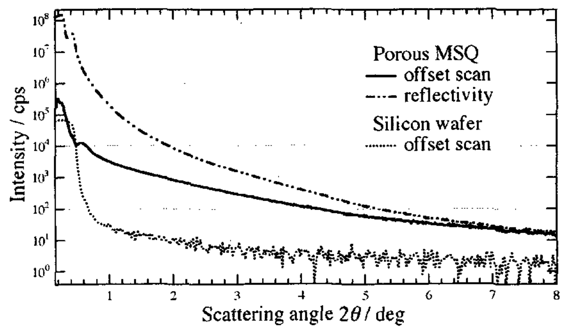

Fig. 3. Diffuse scattering pattern obtained by offset scan and reflectivity curves for a porous MSQ film. Offset scan pattern for a bare silicon wafer is also shown for the comparison.

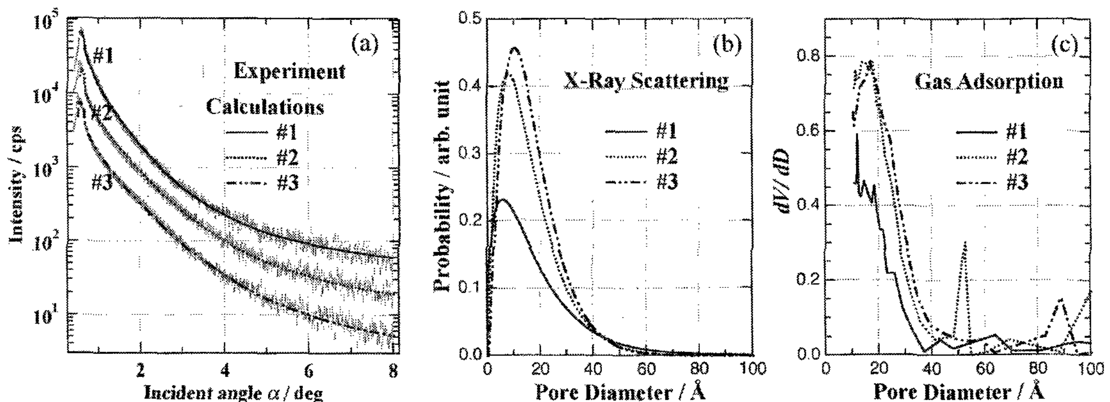

Fig. 4. (a) Experimental and calculated x-ray small angle scattering patterns for the three porous MSQ films. Pore-size distribution of the films obtained by (b) x-ray scattering and (c) N_2 gas adsorption technique.

The sample position was slightly shifted with the angle $\Delta = 0.1°$ from the symmetric $\theta/2\theta$ position (offset scan) to avoid strong specular reflection. This offset angle was selected for obtaining enough separation from the specular reflection. It is depending on the resolution of the measuring system.

The observed reflectivity and small angle diffuse scattering curves for spin-on coated porous methyl silsesquioxane (MSQ) film are shown in Fig. 3. It should be noted that the intensity of specular reflection (reflectivity) is much higher than that of scattering obtained by the offset scan. However, the intensity of offset scan data for the MSQ film is still much higher than that from a bare silicon wafer. This shows that the scattering from the pore is clearly detected.

We compared three spin-on MSQ films #1, #2, and #3 having different dielectric constants by the present technique.

The pore size distributions in the films were determined by comparing experimental and calculated offset-scan curves, and by optimizing the size parameters by least-squares analysis. The observed and calculated scattering patterns and the resultant pore-size distributions by using the optimized parameters are shown in Fig. 4. The pore-size distributions are normalized by the x-ray scattering intensities. The higher scattering intensity indicates higher porosity. In the same figure, we also show the pore-size distributions obtained by N_2 gas adsorption technique. Extremely small pores (diameter $D < 1$ nm) could not be analyzed by the latter technique, because the Kelvin equation is not applicable for such small pores. A reasonable agreement between these two techniques was obtained in the region of $D > 1$ nm.

Diffuse scattering from the film surface sometimes interfere with the scattering by the pores in the film. In such a case, we have to estimate the contribution of the former. It can be calculated based on the equation (10), whereas the parameters of surface roughness σ, ξ, and h are known. In order to estimate these parameters, we have measured rocking scan patterns at several 2θ positions in addition to the offset scan. From these data, we could estimate not only the pore parameters but also the above surface roughness parameters. Typical examples are shown in Fig. 5. The obtained surface parameters are $\sigma = 1.6$ nm, $\xi = 15$ nm, and $h = 0.3$. We could see the contribution of the surface scattering was dominant only at the regions of very low incident and exit angles.

4. CONCLUSION

We have been studied the elements of quantitative analysis for the data of grazing incidence x-ray scattering. Reflection and refraction at the surface and interface is considered by distorted wave Born approximation, and appropriate structural model of the nanostructure has been introduced. Furthermore, we can

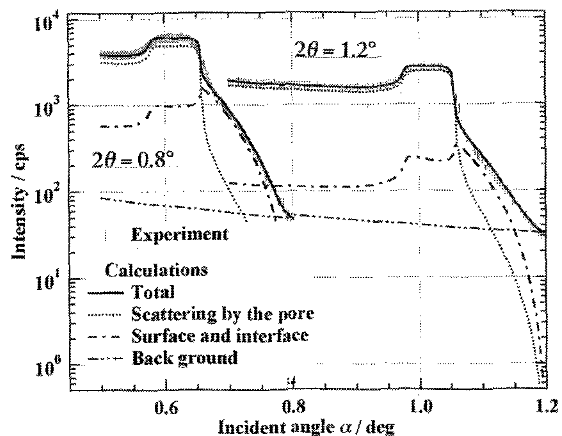

Fig. 5. Rocking scan pattern at $2\theta = 0.8°$ and $1.2°$. The contribution from the pore and surface diffuse scattering are compared.

estimate the contribution of diffuse scattering at the film surface. The present method has been applied for determining pore-size distribution in porous low-κ films and the results were in well accord with that from the gas adsorption technique.

The present technique is also useful for determining the size of particles formed in thin films. For example, magnetic materials, such as nickel granular films, the particle size is critical for the magnetic properties of the films. Other example is silicon nanopareticles in silica matrix film, which show characteristic luminescent spectra dependent on the size of the particles.

For analyzing multilayer films, however, we must optimize lot of structural parameters of not only inside the film but also surface and interfaces. In such a case, it is better to use more scattering data, e.g. $q_{//}$ scan shown in Fig. 1.

References

[1] L. I. Schiff, *Quantum Mechanics*, McGraw-Hill, (1968).
[2] S. K. Sinha, E. B. Sirota, S. Garoff, and H. B. Stanley, *Phys. Rev.* **B38**, 2297 (1988).
[3] V. Holy, J. Kubena, I. Ohlidal, K. Lischka, and W. Plotz, *Phys. Rev.* **B47**, 15896 (1993).
[4] R. Lazzari, *J. Appl. Cryst.* **35**, 406 (2002)
[5] W. L. Wu, W. E. Wallance, E.K. Lin, G. W. Lynn, C. J. Glinka, E. T. Ryan, and H. M. Ho, *J. Appl. Phys.* 87, 1193 (2000).
[6] K. Omote, Y. Ito, S, Kawamura, *Appl. Phys. Lett.* 82, 544 (2003).
[7] K. Omote and J. Harada, *Adv. X-Ray Anal.* 43, 192 (2000).
[8] M. Shuster and H. G¨øebel, *J. Phys.* D28, A270 (1995).

(Received July 21, 2003; Accepted August 21, 2003)